Materials Transactions, Vol. 43, No. 4 (2002) pp. 727 to 734

Non-Destructive Evaluation of Fatigue Damage in Type 316 Stainless Steel Using Positron Annihilation Lineshape Analysis

Yasuhiro Kawaguchi[1], Noriko Nakamura[2] and Satoru Yusa[2]

[1]*Institute of Nuclear Technology, Institute of Nuclear Safety System, Inc., Mihama-cho 919-1205, Japan*
[2]*Research Laboratory, Ishikawajima-Harima Heavy Industries Co., Ltd., Tokyo 135-8732, Japan*

We applied positron annihilation lineshape analysis for non-destructive evaluation of fatigue stored in type 316 stainless steel, mainly used in primary water lines of pressurized water reactors (PWR). Using ^{68}Ge as a positron source, an energy spread of annihilation gamma ray peaks from stainless steel specimens was measured. After preparing stress- and strain-controlled fatigue specimens, we investigated the relation between fatigue life and a non-destructive parameter of lineshape analysis defined as the S-parameter and compared the microstructure of the fatigue specimens with the S-parameter. As a result, there was good correlation between the S-parameter and fatigue life; the S-parameter increased with dislocation density monotonically. The relation between the S-parameter and fatigue life in stress-controlled fatigue differed from that in strain-controlled fatigue. The S-parameter increased faster in early stage of the latter than in the former. In stress-controlled fatigue, the change in the S-parameter did not depend on stress amplitude in the range of ratio to yield stress under 0.9. In the strain-controlled fatigue, the change in the S-parameter did not depend on strain amplitude in the range from 0.25 to 0.31%. However, when stress amplitude or strain amplitude became higher, the change in the S-parameter increased largely in the early stage of the fatigue life. We demonstrated systematic data to evaluate the fatigue damage in type 316 stainless steel.

(Received January 11, 2002; Accepted February 26, 2002)

Keywords: *fatigue, non-destructive evaluation, positron annihilation, annihilation gamma ray, type 316 stainless steel, S-parameter*

1. Introduction

More than thirty years have passed since light water type nuclear power stations were commissioned. It is considered that component materials forming plant facilities have undergone secular changes through their long time operations. For this reason, inspections such as penetrant testing, ultrasonic test, and eddy-current test are conducted with the aim of detecting deterioration before functional failure of nuclear power station components occurs.

In this study, attention was focused on positron annihilation analysis as a means for non-destructively detecting and evaluating symptoms of material deterioration due to fatigue accumulated in stainless steel piping of nuclear power plants long before cracks occur. Positron annihilation analysis provides a method of measuring Doppler broadening and space distribution of gamma rays generated as a result of the annihilation of positrons generated from an accelerator or radioisotopes through the formation of pairs with electrons in a material; it also serves as a method of measuring the time distribution before positrons disappear. The method is known to be sensitive to micro structural changes such as vacancies and dislocations due to plastic deformation long before cracks occur.[1–3] In this study, which was aimed ultimately at enabling evaluation of fatigue damage in nuclear plant piping in the field, we adopted the Doppler broadening method, a method for measuring energy broadening of annihilation gamma rays, because of its simple measurement system.

Although several attempts have been made to measure plastic deformation and fatigue damage for some kinds of materials by using the Doppler broadening method,[4–7] systematic data have not been evaluated. In this study, we prepared specimens by applying fatigue to type 316 stainless steel, widely used in nuclear power stations, measured Doppler broadening using positron annihilation analysis, and examined the feasibility of evaluating fatigue on the basis of the analysis. Hereinafter we describe the positron annihilation analysis by means of the Doppler broadening method as positron annihilation lineshape analysis. We also elaborately investigated the relationship between non-destructive evaluation parameters and fatigue life ratios to evaluate degrees of fatigue damage. We also observed microstructures of the same specimens for comparison with the results obtained from positron annihilation lineshape analysis. In this paper, data obtained from measurement of fatigue specimens with high stress amplitude (270 MPa) and those with high strain amplitude (0.34 to 0.50%) were added to the results presented thus far[8] to summarize all of the data.

2. Experimental Procedure

2.1 S-parameter measurement of positron annihilation

If lattice defects such as dislocations and vacancies exist in materials, conduction electrons ooze into the lattice defects. Then the lattice defects are negatively charged. That is, the absence of metal ions makes such defects negatively charged. This in turn causes positively charged positrons to be attracted to the lattice defects, increasing the proportion of positron annihilation with conduction electrons. In other words, lattice defects in materials provide annihilation sites for positrons. Therefore, as the number of lattice defects increases, the proportion of annihilation with conduction electrons increases. With electrons in materials divided into core electrons and conduction electrons, the energy distribution of gamma rays generated as a result of the annihilation of positrons with conduction electrons has a narrower, sharper peak than the one observed when positrons are annihilated with core electrons.[9] Therefore, as the number of lattice defects, such as dislocations, increases in materials due to fatigue, the proportion of annihilation with conduction electrons increases. Then, the

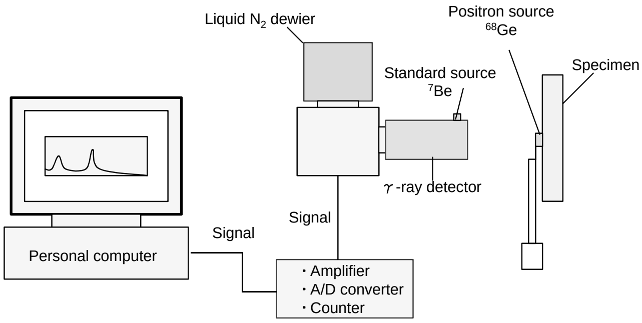

Fig. 1 Positron annihilation lineshape analysis system.

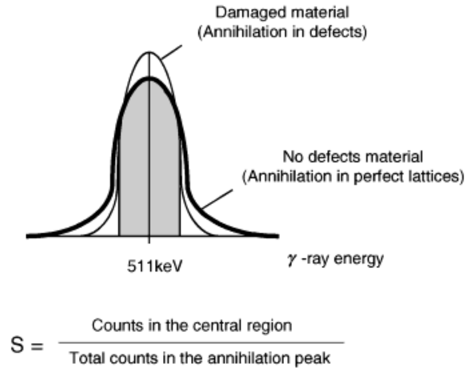

Fig. 2 Definition of S-parameter.

energy distribution of annihilation gamma rays becomes narrower and sharper.

Figure 1 shows the positron annihilation lineshape analysis system (AEA Technology, model PALA-2) we used for the experiment. The system consists of a high resolution intrinsic Ge gamma ray detector (whose resolution is represented by $FWHM = 1.75$ keV for gamma rays with energy of 1.332 MeV from ^{60}Co; the system includes a liquid nitrogen Dewier for cooling the detector), a pre-amplifier, a high voltage power supply, a counting unit (consisting of a main amplifier, an analog-to-digital converter, and a counter), an analyzing unit, a positron source, and other components.

In the present study, ^{68}Ge, with radioactivity of about 740 kBq and 1.48 MBq, was used as the positron source. Having high energy (1.9 MeV maximum), a positron from ^{68}Ge generated by this electron capture diffuses over a range extending relatively deep into a specimen (up to about 250 µm). The positron source was integrated with a strapped joint. During the measurement, positrons generated on the opposite side of the strapped joint were emitted to the specimen. The gamma rays generated as a result of annihilation of electron-positron pairs in the specimen were detected by the gamma ray detector located in front of the specimen and positron source, with the detector output amplified and digitized to be analyzed by a personal computer. When a positron source with stronger intensity was used, a lead collimator (30 mm thick, 14 mm detection hole diameter) was placed between a specimen and the gamma ray detector to adjust the intensity of annihilation gamma rays. A measurement time per one point was about six minutes. Signals detected during a measurement session were analyzed on the spot to calculate an S-parameter showing the degree of broadening of the energy peak exhibited by annihilation gamma rays. As shown in Fig. 2, an S-parameter was defined by the ratio of the number of counts at the center of the energy peak of the annihilation gamma rays (range, 511 ± 0.89 keV) to the number of counts for the entire range (range, 511 ± 14.83 keV). As number of lattice defects increases, the proportion of annihilation with conduction electrons increases, with the width of energy distribution of gamma rays decreasing and hence the peak of the distribution becoming sharper. Therefore the S-parameter increases. In positron annihilation lineshape analysis, we made five or more measurements on a specimen and averaged the values to determine the S-parameter for that specimen.

2.2 Preparation of specimens

Table 1 shows the chemical compositions, solid solution heat treatment conditions, and base metal shapes of the type 316 stainless steel fatigue test materials, while Table 2 shows the mechanical properties of those materials. As shown in Fig. 3, the rod-shaped specimens made using these materials were subjected to the fatigue tests under the following conditions at ambient temperature. After machining, the parallel portions of a specimen were longitudinally ground to the fineness equivalent to finish by #1000 emery paper.

The fatigue test was conducted in the atmosphere at ambient temperature under perfect tension and compression axial stress control or strain control. In the stress-controlled test, sine waves (frequencies of 1.7 Hz and 2 Hz) were applied; while in the strain-controlled test choppings (strain rate of 0.4%/sec) or sine waves (frequency of 1 Hz) were applied. Table 3 shows the test conditions for individual materials.

First, fatigue tests were continued until the specimens were broken to determine the number of cycles to fracture N_f; the test conditions were stress amplitude exceeding 200 MPa for the stress-controlled test and strain amplitude exceeding 0.25% for the strain-controlled test, respectively. Following this test, partway cycle-repeated specimens were prepared that corresponded to several values of N/N_f, with N denoting the number of cycles and N/N_f the fatigue life ratio. For the next tests where the stress amplitude was not more than 200 MPa, specimens with $N = 10^5$ cycles were prepared that were intended for six test conditions corresponding to amplitudes from 100 to 200 MPa at 20 MPa intervals. On the basis of the results on these, three conditions (120, 180, and 200 MPa) were selected and specimens with various numbers of cycles were prepared.

In addition, specimens with mixed degrees of fatigue were prepared such that, after being subjected to a fixed number of fatigue cycles at stress amplitude of 230 MPa in a stress-controlled test, were subjected to fatigue with stress amplitudes other than 200 MPa, 240 MPa, and 250 MPa. Furthermore, in the combination of amplitudes of 230 MPa and 200 MPa, specimens that were subjected to a reversed order of stress amplitude application, namely first to 200 MPa and then 230 MPa, were prepared.

These specimens were cut in the center as shown in Fig. 4 and subjected to positron annihilation lineshape analysis and micro structural observation through a transmission electron microscope (TEM).

Table 1 Chemical composition of type 316 stainless steel test specimens (mass%).

Specimen	C	Si	Mn	P	S	Ni	Cr	Mo	Solution heat treated	Base metal size (mm)
JIS	MAX 0.08	MAX 1.00	MAX 2.00	MAX 0.045	MAX 0.030	10.00 /14.00	16.00 /18.00	2.00 /3.00	1010°C /1150°C	—
A	0.05	0.42	1.75	0.034	0.006	10.30	16.65	2.08	1060°C ×2 h WQ	Pipe: $\phi 216.3 \times {}^{t}23 \times {}^{l}3000$
BA	0.05	0.46	1.50	0.022	0.0005	13.15	16.35	2.21	1060°C ×10 min WQ	Steel bar: $\phi 25 \times {}^{l}1000$
N	0.05	0.32	1.36	0.040	0.027	10.25	16.92	2.00	1050°C ×5 min WQ	Steel bar: $\phi 25 \times {}^{l}1000$
P	0.06	0.50	1.66	0.032	0.002	12.99	16.30	2.08	1050°C ×2 h WQ	Pipe: $\phi 216.3 \times {}^{t}18.2 \times {}^{l}6000$
R	0.05	0.30	1.38	0.035	0.025	10.00	16.84	2.02	1050°C ×5 min WQ	Steel bar: $\phi 25 \times {}^{l}1000$

Table 2 Mechanical properties of type 316 stainless steel test specimens.

Specimen	Yield stress (MPa)	Tensile stress (MPa)	Elongation (%)
JIS	MIN 205	MIN 520	MIN 40
A	264	610	64.3
BA	216	563	61.7
N	288	593	58.0
P	284	559	71.0
R	294	602	55.0

Table 3 Fatigue test conditions.

Specimen	Control	Amplitude	Load pattern	Frequency (Speed)
A	stress	100, 120, 140, 160, 180, 200, 230 (MPa)	sine wave	2 Hz
BA	stress	200, 230 (MPa)	sine wave	2 Hz
N	stress	230, 240, 250 (MPa)	sine wave	2 Hz
	strain	0.25, 0.28, 0.34 (%)	sine wave	1 Hz
P	stress	220 (MPa)	sine wave	1.7 Hz
	strain	0.31 (%)	chopping	0.4%/sec
R	stress	270 (MPa)	sine wave	2 Hz
	strain	0.40, 0.50 (%)	sine wave	1 Hz

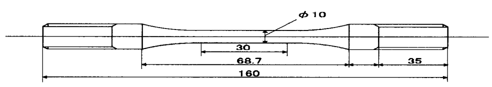

Fig. 3 Configuration of fatigue test specimen.

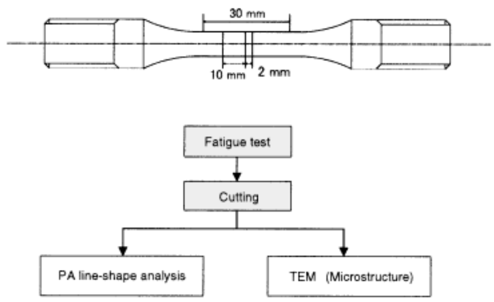

Fig. 4 Evaluation flow of fatigue specimen.

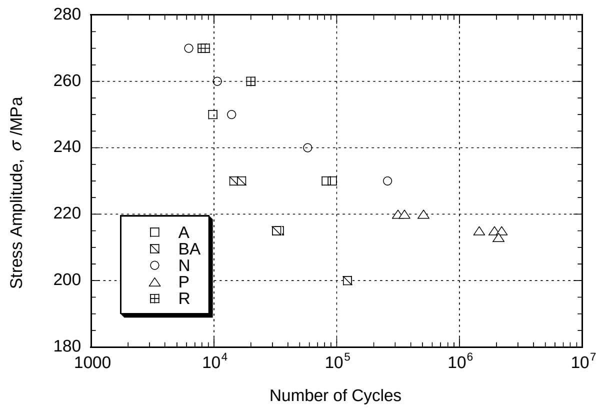

Fig. 5 Number of cycles to fracture of specimens in stress-controlled fatigue.

3. Results and Discussion

3.1 Results of the fatigue test

Figure 5 shows the number of cycles to fracture obtained in the fatigue test under stress control, while Fig. 6 shows the same under strain control. As a result of the stress-controlled test, BA materials with lower yield stress (0.2% proof stress) exhibited lower fatigue strength than other materials did. Materials other than BA exhibited about the same fatigue strength as the fatigue strength of type 316 stainless steel subjected to the rotary bending fatigue test.[10] In the strain-controlled test, material P, which exhibits lower tensile strength, exhibited slightly lower fatigue strength than materials N and R.

3.2 Results of the microstructural observation

Figure 7 shows the result of TEM observation of microstructures after stress-controlled fatigue at stress amplitude of 220 MPa, while Fig. 8 shows it after strain-controlled fatigue at strain amplitude of 0.31%. Having been subjected to solid solution heat treatment at temperatures above 1000°C, the type 316 stainless steel exhibited fewer defects like dislocations in the microstructure at the time of delivery (namely with zero fatigue life ratio), and no precipitates.

At a fatigue life ratio of 1%, an increase in dislocations was observed; the dislocations were locally clustered and entangled. The dislocations were uniformly oriented in a grain. The change in the microstructure due to fatigue was similar to that observed in fatigue-based dislocation structures in austenite steel.[11] As fatigue progressed, dislocations proliferated, with the dislocation density becoming substantially large at a fatigue life ratio of 100%. However, cell structures, which are frequently observed near a point close to fractures after cycles are repeated,[11] were not observed; ours were maze-like rather than cell-like.

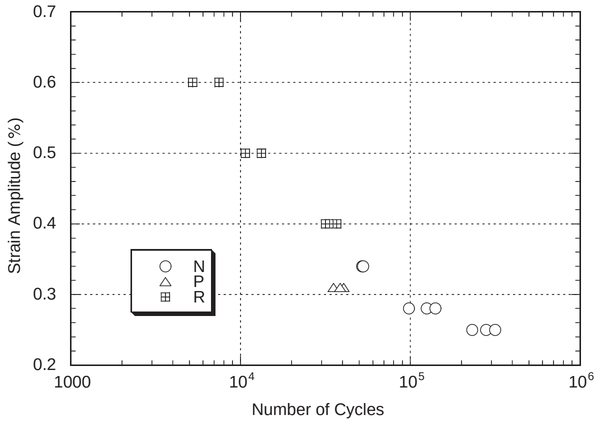

Fig. 6 Number of cycles to fracture of specimens in strain-controlled fatigue.

The comparison of microstructures at a fatigue life ratio of 1% between the stress- and the strain-controlled test revealed a higher dislocation density with the strain-controlled test, indicating that damage at an early stage of strain-controlled fatigue was greater.

3.3 Results of positron annihilation lineshape analysis

Figure 9 shows the relationship between the fatigue life ratio and the S-parameter for all stress-controlled fatigue specimens subjected to stress amplitude of 200 MPa or more. The change in the S-parameter shown in the Y-axis means the increase in the value from standard material (type 316 stainless steel) with fatigue life ratio 0%. Figure 9(a) shows plots for each material using stress amplitudes as parameters, while Fig. 9(b) shows plots for each material using the ratios of stress amplitude σ to yield stress σ_y of the material concerned as parameters. The S-parameter increased with the fatigue life ratio; the tendency of the S-parameter to increase did not differ with stress amplitudes in the lower range (ratio to yield

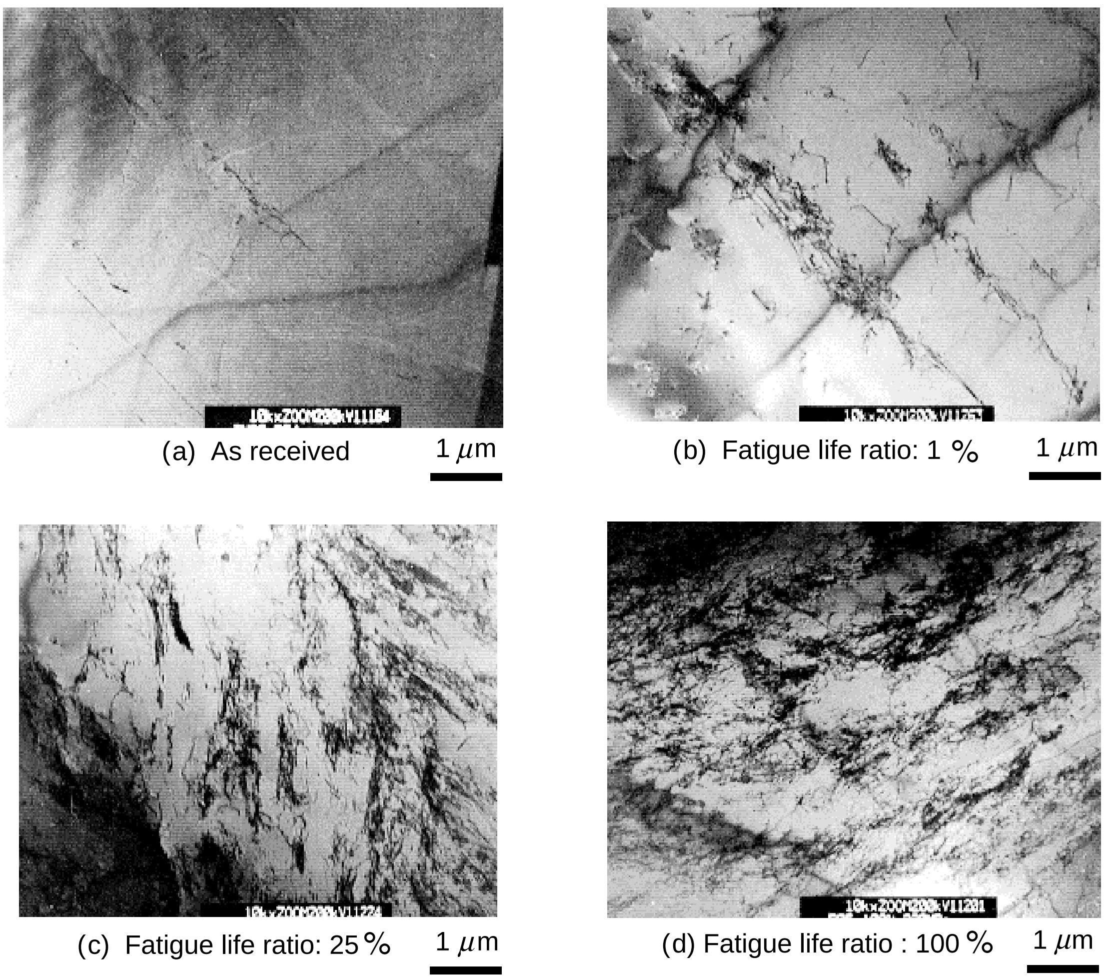

Fig. 7 TEM micrographs of stress-controlled fatigue specimens (Stress amplitude: 220 MPa).

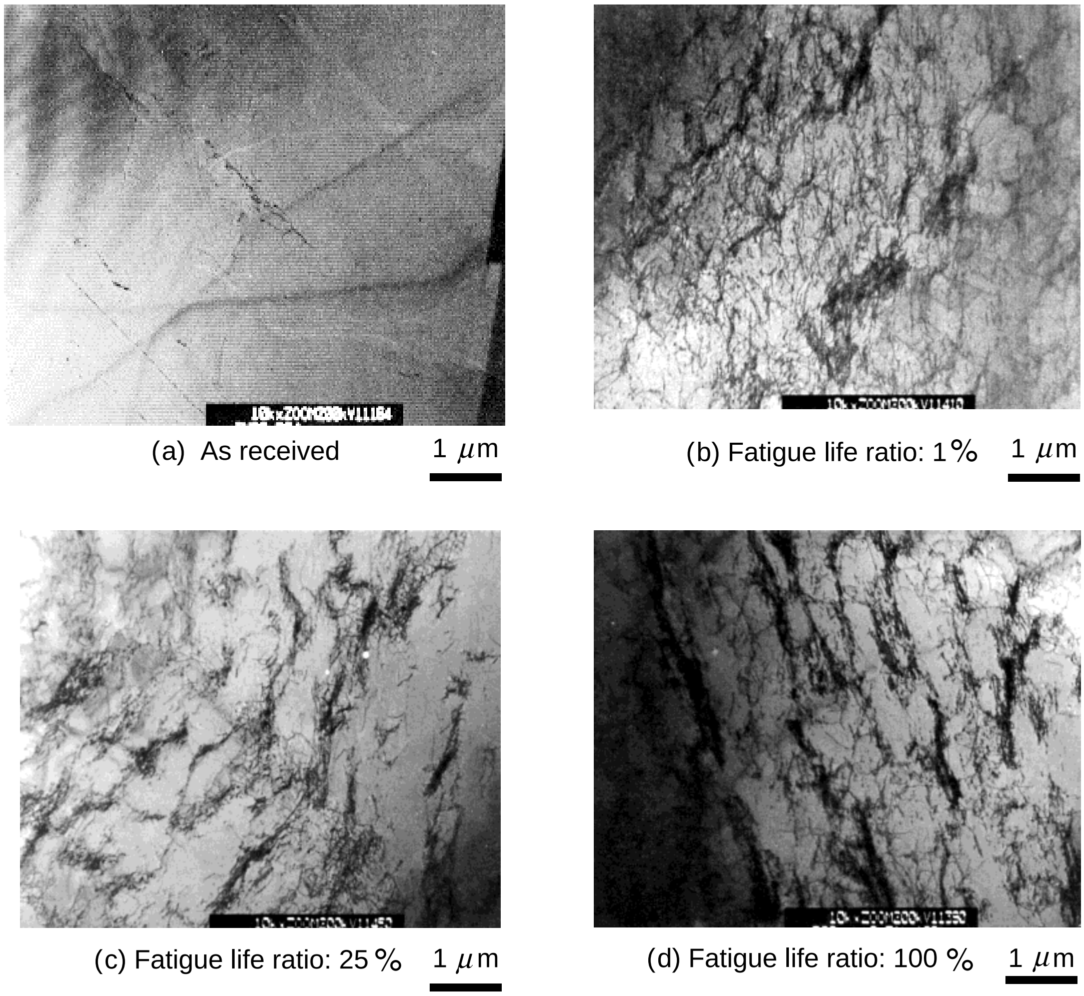

Fig. 8 TEM micrographs of strain-controlled fatigue specimens (Strain amplitude: 0.31%).

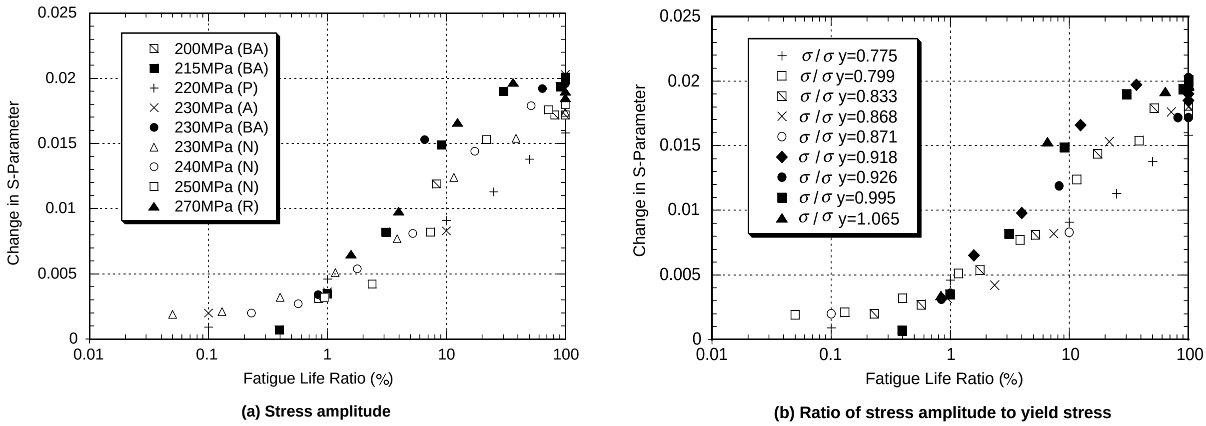

Fig. 9 Relationship between fatigue life ratio and change in S-parameter in stress-controlled fatigue.

stress equal to or less than 0.9), but a sharp increase in the S-parameter occurred in the course of fatigue in a higher stress amplitude range (ratio to yield stress equal to or more than 0.9). In both cases, the amount of change in the S-parameter at the end of fatigue fell between 0.016 and 0.021.

Figure 10 shows the relationship between the stress amplitude and the change in the S-parameter for material A subjected to 10^5 cycles of fatigue at low stress amplitude. For stress amplitude below 180 MPa, the S-parameter changed a little, while it increased remarkably for stress amplitude exceeding 200 MPa.

Figure 11 shows the relationship between the cycles and the change in the S-parameter at low stress amplitude below 200 MPa for material A. For stress amplitude below 180 MPa, the S-parameter tended to increase little with the cycles, while at stress amplitude of 200 MPa, it exhibited a slight tendency

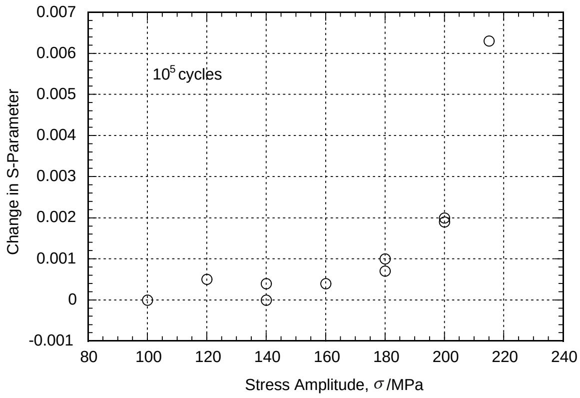

Fig. 10 Results of PA measurement of 10^5 cycles fatigued specimens.

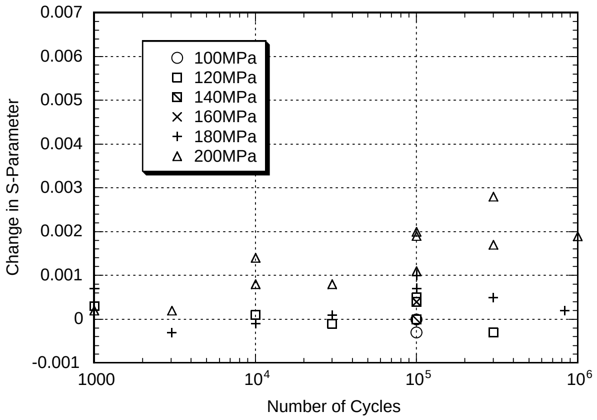

Fig. 11 Results of PA measurement of fatigued specimens with below 200 MPa stress amplitude.

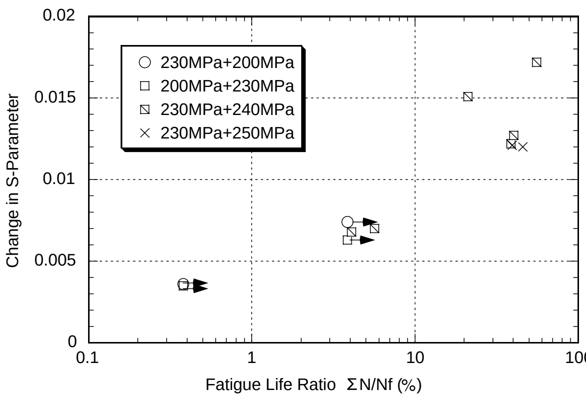

Fig. 12 Results of PA measurement of fatigued specimens with mixed stress amplitude.

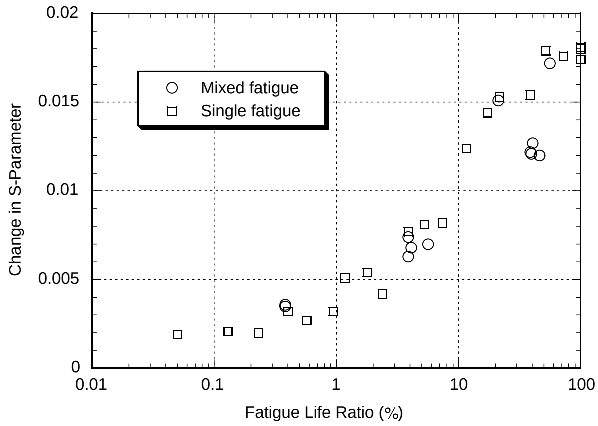

Fig. 13 Comparison between fatigue with mixed stress amplitude and fatigue with single stress amplitude.

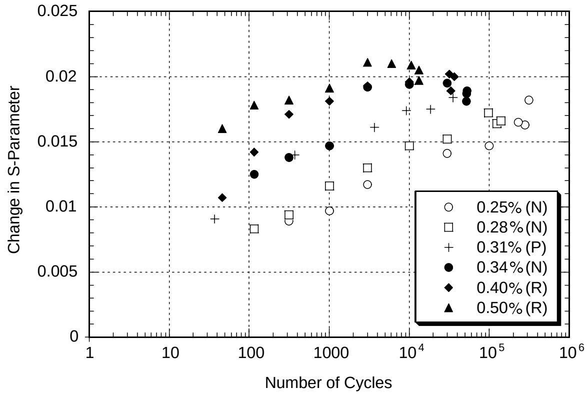

(a) Relationship between number of cycles and change in S-parameter

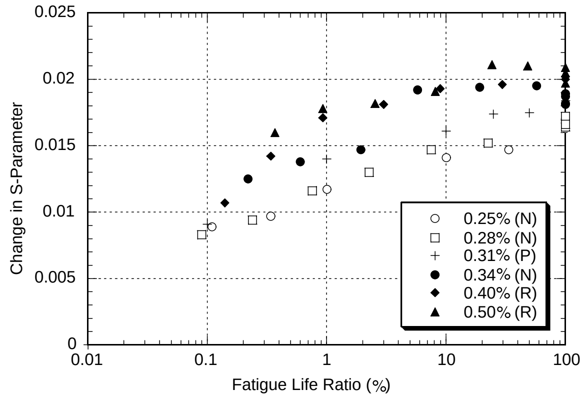

(b) Relationship between fatigue life and change in S-parameter

Fig. 14 Results of PA measurement in strain-controlled fatigue.

to increase, though accompanied by variations.

For material N, Fig. 12 shows the relationship between the fatigue life ratio and the change in the S-parameter in the mixed fatigue test in which the fatigue due to stress amplitude of 230 MPa was mixed with fatigue due to another stress amplitude value. The fatigue life ratio was arranged in the form of $\Sigma N_i/N_{fi}$ according to Miner's law,[12] where N_{fi} denotes the fatigue life resulting from the independent repetition of stress amplitude of σ_i and N_i the number of cycles at the stress amplitude of σ_i.

The figure also shows two cases in which the order of applying different stress levels was changed: in one of them, the stress amplitude was decreased (from 230 to 200 MPa) while in another the stress amplitude was increased (from 200 to 230 MPa). Expressed using Miner's law, the fatigue life ratio in mixed fatigue did not depend on the combination of stress amplitudes; the S-parameter tended to increase with the fatigue life ratio as in single stress amplitude. In addition, changing the order of applying different stress amplitudes hardly changed the S-parameter.

Figure 13 shows both the change in the S-parameter observed with the mixed fatigue shown in Fig. 12 and the change in the S-parameter in single stress amplitude for material N. In the fatigue life ratio range between 40 and 50%, materials subjected to mixed fatigue exhibited lower S-parameters than those subjected to single fatigue; however, both showed about the same tendency. These observations suggest the possibility of evaluating fatigue damage due to mixed stress on the basis of the change in the S-parameter as in the case of single stress amplitude if fatigue damage is expressed in the Miner's law-based fatigue life ratio.

Figure 14 shows the relationship between the number of cycles made under the strain-controlled fatigue condition in the range from 0.25 to 0.50% and the change in the S-parameter and that between the fatigue life ratio and the change in the S-parameter. Also, under the strain control condition, the greater the strain amplitude was, the larger the amount of change there was in the S-parameter associated with the number of cycles. The relationship between the fatigue life ratio and the S-parameter was little affected by strain amplitude in low strain amplitude range of 0.25 to 0.31%. The S-parameter similarly increased with the fatigue life ratio. However, an increase in strain amplitude (0.34% or more) tended to increase the S-parameter in the course of the fatigue. In both cases, the amount of change in the S-parameter at the end of fatigue fell between 0.017 and 0.021.

When the relationship between the fatigue life ratio and the S-parameter under strain control was compared with that obtained under stress control, it was seen that the amount of change in the S-parameter under strain control was higher at the early stage of fatigue (for fatigue life range of 0.1 to 10%). As shown in the TEM micrographs of the specimens in Figs. 7 and 8, the dislocation density of the strain-controlled specimen with 1% fatigue life ratio was greater than that of the stress-controlled one. This suggests that the higher dislocation density of the strain-controlled specimen was due to a greater degree of material damage at the early stage of fatigue and it increased the S-parameter at the early stage of strain-controlled fatigue.

The results described above suggest that, to estimate the fatigue life ratio of a material on the basis of the S-parameter, the evaluation method should be changed depending on whether the fatigue applied to the material is stress- or strain-controlled.

For stress-controlled fatigue in a stress range of 200 to 250 MPa, measurement of the S-parameter, though depending on the material fatigue strength, allowed the fatigue life ratio to be estimated regardless of the stress amplitude. For strain-controlled fatigue in a strain amplitude range of 0.25 to 0.31%, measuring the S-parameter allowed the fatigue life ratio to be estimated regardless of the strain amplitude.

A comparison of these results with those obtained from the observation of the microstructures shown in Figs. 7 and 8 suggests that the increase in the S-parameter was related to the increase in the dislocation density and to the entanglement of dislocations. In other words, with the S-parameter sensitive to microstructures such as the behavior of dislocations, it was considered that an increase in the density of dislocations generated by fatigue increased annihilation sites for positrons and thereby led to an increase in the S-parameter. The observation

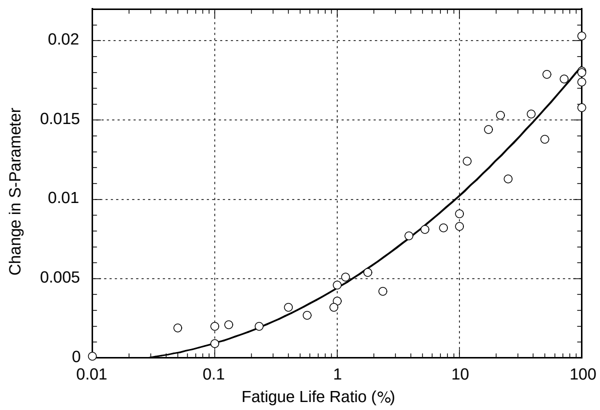

Fig. 15 Fatigue damage evaluation curve for low stress-controlled fatigue.

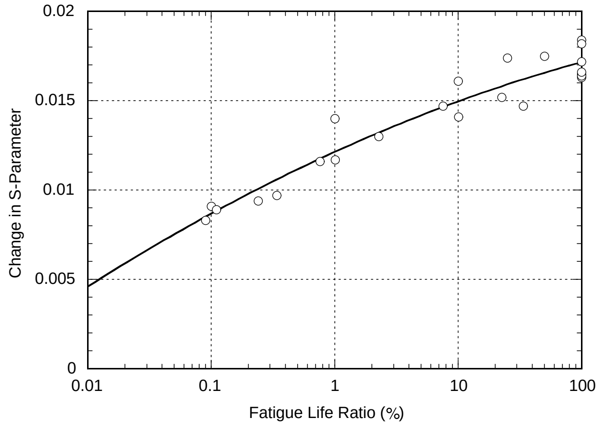

Fig. 16 Fatigue damage evaluation curve for low strain-controlled fatigue.

of microstructures allowed actual structural conditions to be observed in detail and more information to be obtained. However, it is a destructive method and does not allow for easy quantitative evaluation. On the other hand, positron annihilation lineshape analysis provides a non-destructive method that allows microstructural changes to be captured as variations of the S-parameter.

On the basis of the above discussion, we used positron annihilation lineshape analysis to observe Doppler broadening. The observation was made through the S-parameter's behavior accompanying the evolution of fatigue under various strain amplitudes (from 0.25 to 0.50%) and stress amplitudes (from 100 to 270 MPa) in type 316 stainless steel. We confirmed that this technique enabled the degree of fatigue damage to be evaluated.

3.4 Fatigue damage evaluation method

Evaluating the degree of fatigue damage of actual plant material requires that master curves for the S-parameter to the degree of damage (fatigue life ratio) be prepared in advance. Though the relationship between the S-parameter and the fatigue life ratio differed according to whether the fatigue was stress- or strain-controlled, the relationship was independent of the amplitude for fatigue under lower stress amplitude (with $\sigma/\sigma_y = 0.9$ or less) or under lower strain amplitude (from 0.25 to 0.31%). It was also observed in the stress-controlled fatigue that, when the degree of fatigue damage was expressed as fatigue life ratio according to Miner's law, even mixed fatigue exhibited the same relationship as in the case of single stress fatigue.

Taking into account the conclusions of the above discussion, the master curves for evaluating the degree of fatigue damage in these amplitude ranges are shown in Fig. 15, for stress-controlled fatigue, and in Fig. 16, for strain-controlled fatigue.

For the evaluation of a fatigue life ratio as an index of the degree of fatigue damage of actual plant material, the master curve to be applied should be selected according to whether the fatigue applied to the portion to be evaluated is stress-controlled fatigue arising from stress like a change in internal pressure and vibration or strain-controlled fatigue arising from thermal stress or the like. By determining the fatigue life ratio corresponding to the change in the S-parameter measured by the method described above, the degree of fatigue can be evaluated.

The correlation coefficients between the master curves and measured values of the S-parameters were 0.979 for stress-controlled fatigue and 0.979 for strain-controlled fatigue, while the unbiased variance of the S-parameter was 2.00×10^{-6} for stress-controlled fatigue and 8.42×10^{-7} for strain-controlled fatigue.[13]

4. Conclusions

Positron annihilation lineshape analysis, noted as a non-destructive technique, was applied to evaluate fatigue damage in type 316 stainless steel, widely used for piping in nuclear power stations. The possibility of evaluating fatigue damage was experimentally investigated. The study results are summarized below:

(1) The measurement of type 316 stainless steel fatigue specimens using positron annihilation lineshape analysis shows that the amount of change in the S-parameter increases with the fatigue life ratio. The tendency differs depending on the fatigue control method; the amount of change in the S-parameter under strain-controlled conditions starts rising at an earlier stage of fatigue than under stress-controlled conditions.

(2) The relationship between the fatigue life ratio and the S-parameter in stress-controlled fatigue is little affected by the stress amplitude in a low stress amplitude region with a ratio of stress amplitude to yield stress of 0.9 or less; in a region with a ratio of stress amplitude to yield stress of 0.9 or more, however, the S-parameter tends to increase remarkably in the course of fatigue evolution. For strain-controlled fatigue, the relationship between the fatigue life ratio and the S-parameter is little affected by the strain amplitude in a region with strain amplitude of 0.31% or less; for strain amplitude as high as 0.34 to 0.50%, however, the S-parameter increases rapidly in the course of fatigue. In both stress-controlled and strain-controlled fatigue, the S-parameter comes to a value between 0.016 and 0.021 at the end of fatigue.

(3) For fatigue due to mixed stress, the relationship between the S-parameter and the fatigue life ratio becomes the same as in single stress when the degree of fatigue damage is expressed using the fatigue life ratio according to Miner's law.

(4) In the range where the stress amplitude is low (ratio of σ/σ_y not more than 0.9) or in the region where the strain amplitude is low (not more than 0.31%), the S-parameter increases monotonically with the increase in the fatigue life ratio independently of the amplitude. Therefore, it is possible to evaluate the degree of fatigue damage independently of the stress or the strain amplitude by applying the S-parameter measured through positron annihilation lineshape analysis to the master curves.

REFERENCES

1) P. Hautojarvi, ed., A. Dupasquier, P. Hautojarvi, M. J. Manninen, P. E. Mijnarends, R. M. Nieminen, A. Vehanen and R. N. West: *Positrons in Solid*, (Springer-Verlag, 1979) pp. 1–23.
2) G. Brauer, L. Liszkay, B. Molnar and R. Krause: Nuclear Engineering and Design **127** (1991) 47–68.
3) M. Hasegawa: Materia Japan **35** (1996) 93–102.
4) A. E. Hughes: Materials in Engineering. **2** (1980) 34–40.
5) M. Uchida, Y. Ohta, N. Nakamura and K. Yoshida: Application of positron annihilation lineshape analysis to fatigue damage and thermal embrittlement for nuclear plant materials, (Proceedings of the 13th International Conference on NDE in the Nuclear and Pressure Vessel Industries, 1995) pp. 349–353.
6) N. Maeda, N. Nakamura, M. Uchida, Y. Ohta and K. Yoshida: Nuclear Engineering and Design **167** (1996) 169–174.
7) K. Miyahara, K. Sato, K. Nagai and M. Hasegawa: CAMP-ISIJ **13** (2000) 1388.
8) Y. Kawaguchi and N. Nakamura: J. Japan Inst. Metals **65** (2001) 835–842.
9) Y. Otsuki, ed., K. Kawarabasi, S. Tanikawa and K. Yosida: Butsurigaku Saizensen **5** (1983) 75–80.
10) JSMS, ed.: *Data Book on Fatigue Strength of Metallic Materials*, **1** (JSMS, 1982) pp. 112–114.
11) S. Kocanda: *Fatigue Failure of Metals*, (T. Yokobori, ed., H. Ishii, M. Tanaka. trans., Gendairikogakusha, 1981) pp. 180–184.
12) JIM, ed.: *Kinzoku Binran*, (Maruzen, 1990) pp. 387.
13) Y. Yoshizawa: *Atarashii Gosaron*, (Kyoritsu Shuppan, 1990) pp. 180–188.